Transp Porous Med (2017) 117:367–383
DOI 10.1007/s11242-017-0838-8

A New Non-Darcy Flow Model for Low-Velocity Multiphase Flow in Tight Reservoirs

Yi Xiong[1] · Jinbiao Yu[2] · Hongxia Sun[2] · Jiangru Yuan[3] · Zhaoqin Huang[4] · Yu-shu Wu[1]

Received: 1 April 2016 / Accepted: 9 February 2017 / Published online: 23 February 2017

Abstract The pore and pore-throat sizes of shale and tight rock formations are on the order of tens of nanometers. The fluid flow in such small pores is significantly affected by walls of pores and pore-throats. This boundary layer effect on fluid flow in tight rocks has been investigated through laboratory work on capillary tubes. It is observed that low permeability is associated with large boundary layer effect on fluid flow. The experimental results from a single capillary tube are extended to a bundle of tubes and finally to porous media of tight formations. A physics-based, non-Darcy low-velocity flow equation is derived to account for the boundary layer effect of tight reservoirs by adding a non-Darcy coefficient term. This non-Darcy equation describes the fluid flow more accurately for tight oil reservoir with low production rate and low pressure gradient. Both analytical and numerical solutions are obtained for the new non-Darcy flow model. First, a Buckley–Leverett-type analytical solution is derived with this non-Darcy flow equation. Then, a numerical model has been developed for implementing this non-Darcy flow model for accurate simulation of multi-dimensional porous and fractured tight oil reservoirs. Finally, the numerical studies on an actual field example in China demonstrate the non-negligible effect of boundary layer on fluid flow in tight formations.

Keywords Non-Darcy flow · Tight oil reservoirs · Numerical simulation · Buckley–Leverett solution · Boundary layer effect

✉ Yi Xiong
yixiong@chevron.com

[1] Colorado School of Mines, Golden, CO, USA

[2] China Petroleum & Chemical Corp (SINOPEC), Beijing, China

[3] RIPED of PetroChina, Beijing, China

[4] China University of Petroleum (East China), Qingdao, China

1 Introduction

Darcy's law (Darcy 1856) is the exclusive formulation to model subsurface fluid flow in oil and gas reservoirs; it describes a linear relationship between volumetric flow rate (Darcy velocity) and pressure gradient. It is also the fundamental principle for many other applications in oil and gas industry, especially in the areas of well testing analysis and reservoir simulation (Ahmed and McKinney 2011; Aziz and Settari 1979). On the other hand, Darcy's law is only valid for laminar and viscous flow (Ahmed 2006), and any deviations from this linear relation can be defined as non-Darcy flow. It has long been recognized that non-Darcy flow phenomena could exist in many systems involving high flow rate, e.g., CO_2 sequestration (Zhang et al. 2014) and Enhanced Oil Recovery (EOR) system (Wu et al. 2010), and enhanced geothermal system (Wu et al. 2015; Xiong et al. 2013). For example, Forchheimer (1901) extended Darcy's linear form to a quadratic flow equation, and eventually added an additional cubic term to formulate flow at high flow rate in porous media. In addition, many efforts have been added to improve Forchheimer model for fitting larger range of fluid flow with high flow rate (Carman 1997; Ergun 1952; Montillet 2004) and extend it to multiphase conditions (Evans and Evans 1988; Evans et al. 1987). Barree and Conway (2004) proposed a new high-velocity non-Darcy flow model based on experimental results and field observation. It is more general than Forchheimer model since it does not rely on the assumption of a constant permeability. Both of the two non-Darcy flow models, Forchheimer and Barree and Conway, have been widely applied to the numerical studies in oil and gas reservoirs (Xiong 2015), CO_2 sequestration and EOR under high flow rate.

In addition to extensive investigations on high-velocity non-Darcy flow, the nonlinear relationship between volumetric flow rate and pressure gradient is also observed and studied for low-velocity fluid flows. For example, Prada and Civan (1999) introduced the concept of threshold pressure gradient to correct Darcy's law for low-velocity flow where fluids can flow through porous media only if the fluid flowing force is sufficient to overcome the threshold pressure gradient, and they recommend further research to improve correlations of the threshold pressure gradient. Civan (2008) also derived the condition of threshold pressure gradient at which the fluid can flow with a generalized Darcy's law by control volume analysis due to intricate complexity of porous media averaging method (Civan 2002). Gavin (2004) calls the departure from Darcy's law at low fluid velocities as "Pre-Darcy behavior" in petroleum reservoirs and claims that there could be substantial unrecognized opportunities for increasing hydrocarbon recovery. Zeng et al. (2011) designed the experimental equipment to investigate single-phase flow in ultra-low-permeability cores, using capillary flow meter to achieve accurate measurement of fluid volume. Their results confirm that the single-phase flow in ultra-low-permeability cores is not consistent with Darcy's Law. Liu et al. (2015) proposed a phenomenological model for non-Darcy liquid flow in shale and develop an analytical solution to one-dimensional spontaneous imbibition problem that obeys the model. In addition, the low-velocity non-Darcy phenomena are also intensively studied in non-petroleum disciplines. Hansbo (1960, 2001) reported a power function between flux and pressure gradient for water flow in low-permeability clay soil under small values of pressure gradient, which becomes linear if pressure gradient becomes larger. Civan (2013) provided a rigorous derivation of a power-law function based on an empirical gradient law in spontaneous transport in porous media. Swartzendruber (1962) proposed to modify the linear relationship of Darcy's law to an exponential function for water flow in tight soil. Liu (2014) indicated that non-Darcy flow behavior is common in low-permeability media through reviewing studies on water flow in shale formations under the context of nuclear waste disposal.

In this paper, we study non-Darcy flow in low-permeability reservoir through experiments, theoretical analysis, and numerical simulation. The next section presents our experimental results from a single capillary tube, which shows the effect of a boundary layer of fluid in capillary tube on flow behavior. The results from a single capillary tube are then extended to multiple tubes and to multiphase flow in a porous medium. Our empirical formulation from experimental data is a continuous function including both Darcy and non-Darcy flows, and a numerical model has been developed to capture this experiment-based non-Darcy fluid behavior. Finally, we perform a field study with this numerical model for a multi-stage hydraulic fracturing well in a tight oil reservoir.

2 Experimental Results

Researchers have realized that fluid flow in a very small capillary tube consists of body flow and boundary flow through experimental study and theoretical analysis (Huang et al. 2013; Jiang et al. 2011; Xu and Yue 2007). The body flow is the fluid flow not affected by tube wall, and boundary flow is the portion of fluid under the effect of tube wall. The smaller of capillary tube, the larger of boundary flow relatively.

The experiment is performed on a single capillary tube with radius r and the thickness of boundary flow δ shown in Fig. 1a. The experimental method and setup is the same as the work of Xu and Yue (2007) but performed independently, where the thickness of boundary flow is calculated from measured flow rate and pressure gradient along the tube, which is filled with deionized water (see "Appendix" for detailed experimental setup). Our experimental results show an exponential function between the thickness of boundary flow and pressure gradient, described in Eq. (1).

$$\delta = \delta_0 \mathrm{e}^{-c\nabla p} \tag{1}$$

where δ_0 is thickness of static (maximum) boundary flow. We define dimensionless boundary layer as ratio of static boundary layer over tube radius, $\delta_\mathrm{D} = \delta_0/r$. We also introduce a coefficient c, which is a regression parameter to match exponential function. The flow rate then can be derived from Eq. (1) and Hagen–Poiseuille Equation as below.

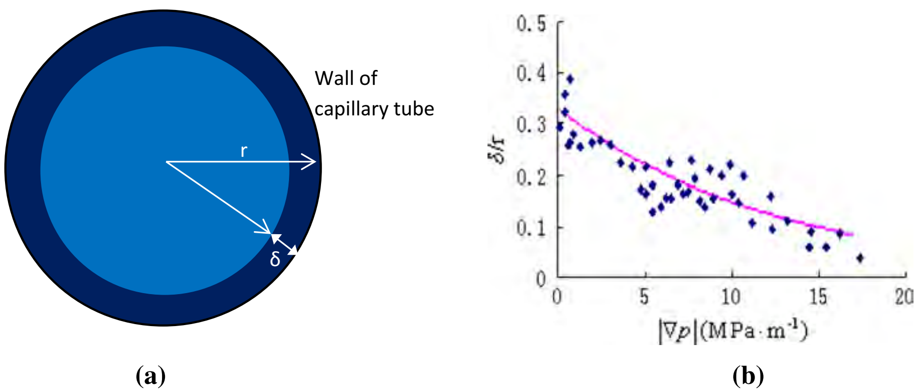

Fig. 1 **a** Flow in capillary tube; **b** relationship between ratio of thickness of boundary flow over tube radius and pressure gradient

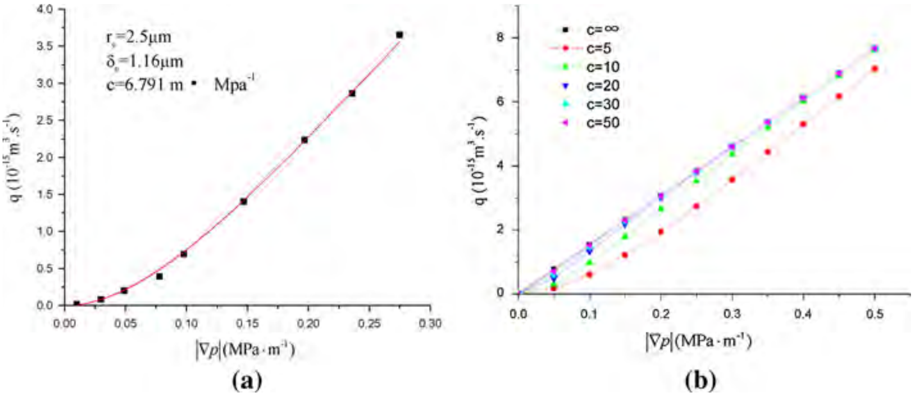

Fig. 2 **a** Flow rate versus pressure gradient from experimental results; **b** the extent of nonlinearity for different values of *c*

$$q = \int_0^{r_0-\delta} v(r) \cdot 2\pi r \mathrm{d}r = \frac{\pi \left(1 - \delta_\mathrm{D} \mathrm{e}^{-c|\nabla p|}\right)^4 r_0^4}{8\mu} |\nabla p| \tag{2}$$

The equation above is a linear function of Hagen–Poiseuille Equation between flow rate and pressure gradient if pressure gradient becomes large:

$$q = \frac{\pi r_0^4}{8\mu} |\nabla p| \tag{3}$$

Again, c and δ_D of Eq. (2) are two parameters determined from experiment results, where δ_D is determined by indirectly measuring the thickness of static boundary δ_0, which is the thickness of boundary layer at minimum pressure gradient. In other words, static boundary δ_0 does not increase anymore as pressure gradient further decrease; c is determined by constructing exponential curve between pressure gradient and corresponding thickness of boundary flow, and c is the exponential coefficient as in Eq. (1).

We performed an experiment in a capillary tube with 2.5 μm radius, and the results show a good agreement with Eq. (2) with the determined c and δ_D values, shown in Fig. 2a. Figure 2b plots the extent of nonlinearity with different c values. A smaller c value gives larger extent of nonlinearity and an infinity value of c essentially gives a linear function.

The single tube experiment-based nonlinear function Eq. (2) can be extended to flow through multiple tubes:

$$Q = \sum_{i=1}^{N} n_i q(r_i) = \sum_{i=1}^{N} n_i \frac{\pi \left(1 - \delta_i \mathrm{e}^{-c_i|\nabla p|}\right)^4 r_i^4}{8\mu} |\nabla p| \tag{4}$$

According to Hagen–Poiseuille Equation, the equivalent form of Eq. (4) for a porous medium can be written as

$$v = \frac{k \left(1 - \delta_\mathrm{D} \mathrm{e}^{-c_\phi|\nabla p|}\right)^4}{\mu} \nabla p \tag{5}$$

where k and μ are absolute permeability and fluid viscosity. Equation (5) is our experiment-based single-phase non-Darcy flow model with non-Darcy terms, related to boundary flow. One big advantage of Eq. (5) is that it is a continuous function describing both Darcy and

Table 1 Values of dimensionless static boundary layer of water and oil phases

Permeability (mD)	δ_D of each phase at different water fractional flows f_w					Average δ_D
0.611		$f_w = 0.877$	$f_w = 0.768$	$f_w = 0.644$	$f_w = 0.456$	
	Water phase	0.348	0.374	0.372	0.389	0.37
	Oil phase	0.374	0.371	0.390	0.349	0.37
2.85		$f_w = 0.942$	$f_w = 0.905$	$f_w = 0.855$	$f_w = 0.724$	
	Water phase	0.291	0.319	0.403	0.352	0.34
	Oil phase	0.321	0.403	0.354	0.289	0.34
10.2		$f_w = 1.0$	$f_w = 0.805$	$f_w = 0.712$	$f_w = 0.624$	
	Water phase	0.115	0.118	0.188	0.123	0.14
	Oil phase	0.124	0.187	0.116	0.153	0.14

non-Darcy flow with a single formulation, with more accuracy on low-velocity flow under small pressure gradient.

Equation (5) can be further extended to multiphase flow through two-phase experiments, which indirectly measure static dimensionless boundary layer by assuming different phases (water or oil) occupy boundary layer under a variety of permeability and water fractional flow. Table 1 summarizes the values of dimensionless boundary layer from two-phase experiments. It shows that δ_D could be different at certain water fractional flow and depends on which phase is treated as boundary fluid. But the difference is quite small for low-permeability rock, and the average values for oil and water phases are actually almost same at different water fractional flows. Therefore, the static boundary layer is only function of permeability and phase independent. The lower permeability rock has a larger value of δ_D; it is physically sound because the lower permeability leads to a smaller flow portion of fluid and relative thicker static boundary layer. Therefore, Eq. (5) can have the multiphase version as Eq. (6).

$$v_\beta = \frac{kk_{r\beta}\left(S_\beta\right)\left(1 - \delta_D e^{-c\phi_\beta \left|\nabla p_\beta\right|}\right)^4}{\mu_\beta} \nabla p_\beta \tag{6}$$

where β can be either water or oil phase. Parameter c describes the degree of nonlinearity between flow rate and pressure gradient, and it is related to both flowing fluid and properties of porous media, such as wettability and pore structures.

3 Analytical Solutions

This section presents the Buckley–Leverett analytical solution (Buckley and Leverett 1942) with gravity effect in porous media in order to obtain some insight into the physics behind two-phase immiscible displacement under this low-velocity non-Darcy flow model. Here, this analytical solution is used to study the oil displacement by water through water injection to vertical column at the top inlet. The vertical column is a homogenous porous medium with initial oil saturation 0.8 and residual water saturation 0.2. Other rock properties for the vertical column are listed in Table 2.

Table 2 Rock and fluid properties for B–L analytical solution

Parameters	Values	Units
Absolute permeability	1.0×10^{-14}	m^2
Porosity	0.1	
Residual water saturation	0.2	
Residual oil saturation	0.2	
Cross section area	1.0	m^2
Water viscosity	1.139×10^{-3}	Pa s
Water density	1000	kg/m^3
Oil density	864	kg/m^3
Water injection rate	0.01728	m^3/day
Brooks–Corey k_r exponent	1.0	

The flow rate of 1D flow with gravity has the following equations for water and oil according to Eq. (6).

$$q_{\mathrm{o}} = -\frac{kk_{\mathrm{ro}}A}{\mu_{\mathrm{o}}}\left(1-\delta_{\mathrm{Do}}\mathrm{e}^{-c_{\phi\mathrm{o}}|\mathrm{d}P_{\mathrm{o}}/\mathrm{d}x+\rho_{\mathrm{o}}g\sin\alpha|\times 10^{-6}}\right)^4\left(\frac{\mathrm{d}P_{\mathrm{o}}}{\mathrm{d}x}+\rho_{\mathrm{o}}g\sin\alpha\right) \tag{7}$$

$$q_{\mathrm{w}} = -\frac{kk_{\mathrm{rw}}A}{\mu_{\mathrm{w}}}\left(1-\delta_{\mathrm{Dw}}\mathrm{e}^{-c_{\phi\mathrm{w}}|\mathrm{d}P_{\mathrm{w}}/\mathrm{d}x+\rho_{\mathrm{w}}g\sin\alpha|\times 10^{-6}}\right)^4\left(\frac{\mathrm{d}P_{\mathrm{w}}}{\mathrm{d}x}+\rho_{\mathrm{w}}g\sin\alpha\right) \tag{8}$$

Buckley–Leverett problem ignores fluid compressibility and capillary pressure. Thus, a governing equation can be written:

$$q_{\mathrm{t}} - q_{\mathrm{w}} - q_{\mathrm{o}} = 0 \tag{9}$$

where q_t is constant total injection rate and q_{w} and q_{o} are flow rates of water and oil, respectively.

Plugging Eqs. (7) and (8) into Eq. (9), we obtain an Equation with one unknown $\mathrm{d}P/\mathrm{d}x$ for a given Sw. Wu (2001) used the similar method to derive Buckley–Leverett solution for Forchheimer non-Darcy flow and proves the pressure gradient and the saturation are interdependent on each other. In other words, Eq. (9) can be solved for $\mathrm{d}P/\mathrm{d}x$ with iterative method for a given S_{w}, and therefore q_{w} and q_{o} can be calculated.

The water fractional flow then can be obtained as below and corresponding fractional flow curve can be plotted.

$$f_{\mathrm{w}} = \frac{q_{\mathrm{w}}}{q_{\mathrm{t}}} \tag{10}$$

The steps to calculate Buckley–Leverett analytical solution are summarized:

- Given a S_{w}
- Obtain $k_{\mathrm{ro}}(S_{\mathrm{w}})$ and $k_{\mathrm{rw}}(S_{\mathrm{w}})$
- Plug all data to Eq. (9)
- Solve $\mathrm{d}P/\mathrm{d}x$ with iterative method (Bi-section is enough because Eq. (9) is monotonic in terms of $\mathrm{d}P/\mathrm{d}x$)
- Plug solved $\mathrm{d}P/\mathrm{d}x$ to Eq. (8) to solve q_{w}
- Calculate f_{w}
- Repeat above steps for another S_{w} and finally build fractional flow curve $f_{\mathrm{w}} = f_{\mathrm{w}}(S_{\mathrm{w}})$

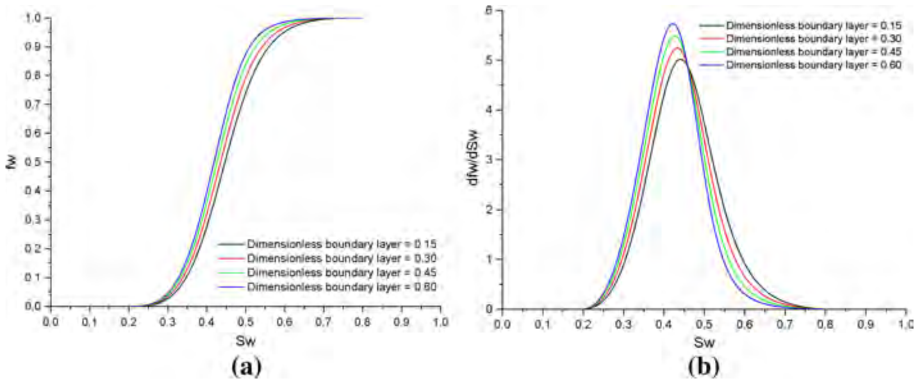

Fig. 3 Fractional flow (**a**) and derivative (**b**) curves for various dimensionless boundary layer values

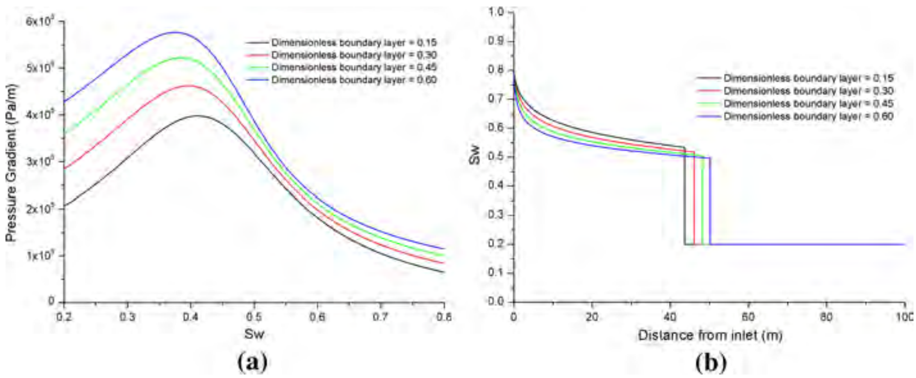

Fig. 4 **a** Pressure gradient as a function of water saturation; **b** saturation profile after 100 days injection

Once the fractional flow curve is built, its derivatives can be calculated and thus the saturation profile can be obtained:

$$x_{S_\mathrm{w}} = \frac{q_\mathrm{t} t}{A\phi}\left(\frac{\partial f}{\partial S_\mathrm{w}}\right)_{S_\mathrm{w}} \tag{11}$$

The non-Darcy parameter in Eq. (6), dimensionless boundary layer δ_D, is studied by construct a variety of analytical solutions with different values of δ_D. Figures 3 and 4 show the results with constant $c_\phi(c_{\phi\_\mathrm{water}=}10.1 c_{\phi\_\mathrm{oil}=}2.1)$ but varied dimensionless boundary layer δ_D. Figure 3 presents the fractional flow and their derivatives with a variety of dimensionless boundary layer; Fig. 4a plots pressure gradient as function of water saturation for maintaining the constant water injection rate; Fig. 4b shows the saturation profile along rock column direction after 100 days water injection.

Figure 4a shows that a larger pressure gradient is required to maintain the given water injection rate and flow rate in the case of a larger dimensionless boundary layer; it can be explained that a larger dimensionless boundary layer results in a smaller portion of flowable fluids (or a larger portion of non-flowable fluids) in a porous medium, and thus a larger drive force is necessary. Figure 4b presents that water (wet) phase front moves further after same period of water injection with a larger dimensionless boundary layer, but it has less water saturation in the places before water front.

4 Numerical Model

A numerical model has been developed based on Eq. (6) and implemented into an existing black oil reservoir simulator MSFLOW (Wu 1998). MSFLOW is a numerical reservoir simulator for modeling three-phase flow of oil, gas, and water in multidimensional porous and fractured reservoirs. The numerical discretization technique used in the MSFLOW code is the integral finite difference method (Narasimhan and Witherspoon 1976; Pruess 1991). The numerical implementation in this paper takes advantages of existing numerical framework of MSFLOW and only modified the flow term according to this new non-Darcy multiphase flow equation. The discrete nonlinear equations of grid block i then can be written:
For gas flow:

$$\begin{aligned}
&\left[\left(\phi S_{\mathrm{o}}\rho_{\mathrm{dg}}+\phi S_g\rho_g\right)_i^{n+1}-\left(\phi S_{\mathrm{o}}\rho_{\mathrm{dg}}+\phi S_g\rho_g\right)_i^{n}\right]\frac{V_i}{\Delta t}\\
&\quad=\sum_{j\in\eta_i}\left(\rho_{\mathrm{dg}}\lambda_{\mathrm{o}}\right)_{ij+1/2}^{n+1}\left(C_{\mathrm{o}}^{\mathrm{nD}}\right)_{ij}\gamma_{ij}\left(\psi_{\mathrm{o}j}^{n+1}-\psi_{\mathrm{o}i}^{n+1}\right)\\
&\qquad+\sum_{j\in\eta_i}\left(\rho_g\lambda_g\right)_{ij+1/2}^{n+1}\gamma_{ij}\left(\psi_{gj}^{n+1}-\psi_{gi}^{n+1}\right)+Q_{gi}^{n+1}
\end{aligned}\tag{12}$$

For water flow:

$$\left[\left(\phi S_{\mathrm{w}}\rho_{\mathrm{w}}\right)_i^{n+1}-\left(\phi S_{\mathrm{w}}\rho_{\mathrm{w}}\right)_i^{n}\right]\frac{V_i}{\Delta t}=\sum_{j\in\eta_i}\left(\rho_{\mathrm{w}}\lambda_{\mathrm{w}}\right)_{ij+1/2}^{n+1}\left(C_{\mathrm{w}}^{\mathrm{nD}}\right)_{ij}\gamma_{ij}\left(\psi_{\mathrm{w}j}^{n+1}-\psi_{\mathrm{w}i}^{n+1}\right)+Q_{\mathrm{w}i}^{n+1}\tag{13}$$

For oil flow:

$$\left[\left(\phi S_{\mathrm{o}}\rho_{\mathrm{o}}\right)_i^{n+1}-\left(\phi S_{\mathrm{o}}\rho_{\mathrm{o}}\right)_i^{n}\right]\frac{V_i}{\Delta t}=\sum_{j\in\eta_i}\left(\rho_{\mathrm{o}}\lambda_{\mathrm{o}}\right)_{ij+1/2}^{n+1}\left(C_{\mathrm{o}}^{\mathrm{nD}}\right)_{ij}\gamma_{ij}\left(\psi_{\mathrm{o}j}^{n+1}-\psi_{\mathrm{o}i}^{n+1}\right)+Q_{\mathrm{o}i}^{n+1}\tag{14}$$

Different from conventional black oil model, non-Darcy coefficients are introduced in above flow equations. For gas flow, non-Darcy coefficient of oil phase is added to flow term of dissolved gas. The non-Darcy coefficient of oil and water phase then can be written as:

$$\left(C_{\mathrm{o}}^{\mathrm{nD}}\right)_{ij}=\left[1-\left(\delta_{\mathrm{D}}^{n+1}\right)_{ij}\mathrm{e}^{-c_{\phi\mathrm{o}}\left|\psi_{\mathrm{o}j}^{n+1}-\psi_{\mathrm{o}i}^{n+1}\right|}\right]^4\tag{15}$$

$$\left(C_{\mathrm{w}}^{\mathrm{nD}}\right)_{ij}=\left[1-\left(\delta_{\mathrm{D}}^{n+1}\right)_{ij}\mathrm{e}^{-c_{\phi\mathrm{w}}\left|\psi_{\mathrm{w}j}^{n+1}-\psi_{\mathrm{w}i}^{n+1}\right|}\right]^4\tag{16}$$

In above equations, ρ_β is the density of phase β at reservoir condition; ρ_{o} is the density of oil excluding dissolved gas and ρ_{dg} is the density of dissolved gas in oil phase both at reservoir conditions. ϕ is the effective porosity of formation; α_β, S_β, ψ_β, Q_β is the mobility, saturation, potential and flow rate of phase β, where mobility and potential are defined:

$$\lambda_\beta=k_{r\beta}/\mu_\beta\tag{17}$$

$$\psi_{\beta i}^{n+1}=P_{\beta i}^{n+1}-\rho_{\beta,ij+1/2}^{n+1}gD_i\tag{18}$$

The subscripts i, j represent grid blocks, and Υ_{ij} is the transmissibility between i and j defined as:

$$\gamma_{ij}=\frac{k_{ij+\frac{1}{2}}A_{ij}}{d_i+d_j}\tag{19}$$

And subscript $ij + 1/2$ represents the connection between two grid blocks; superscript $n + 1$ stands for current time step. All variables are evaluated fully implicitly. Above discretized equations can be written with residual forms, and Newton–Raphson method is used to solve the residual equation system.

The developed numerical model can be generally applied to tight oil reservoirs to study boundary layer-induced non-Darcy effect. The numerical model is also validated against analytical solution for a Buckley–Leverett problem including gravity effect.

5 Validation of Numerical Model

A Buckley–Leverett problem including gravity effect is solved with the developed numerical model, and an analytical solution is derived by above method. The rock and fluid parameters in Table 2 are used to get the fractional flow curve (analytical solution) and the numerical results. Table 3 lists the non-Darcy parameters in the validation example.

The simulation domain is a 1D vertical rock column with 200 m by a uniform block-centered grid consisting of 100 elements. The water is injected at top and a constant pressure is described at 1 bar on the bottom boundary as shown in Fig. 5a. With the input data in Tables 2 and 3, a comparison of water saturation profiles at 100 days of injection, predicted by numerical code and analytical solution, is shown in Fig. 5b. The numerical and analytical results are in good agreement.

Table 3 Non-Darcy parameters in the validation

Parameters	Water	Oil
δ_D	0.14	0.14
c_ϕ	10.1	2.1
Nonlinear exponent	4.0	4.0

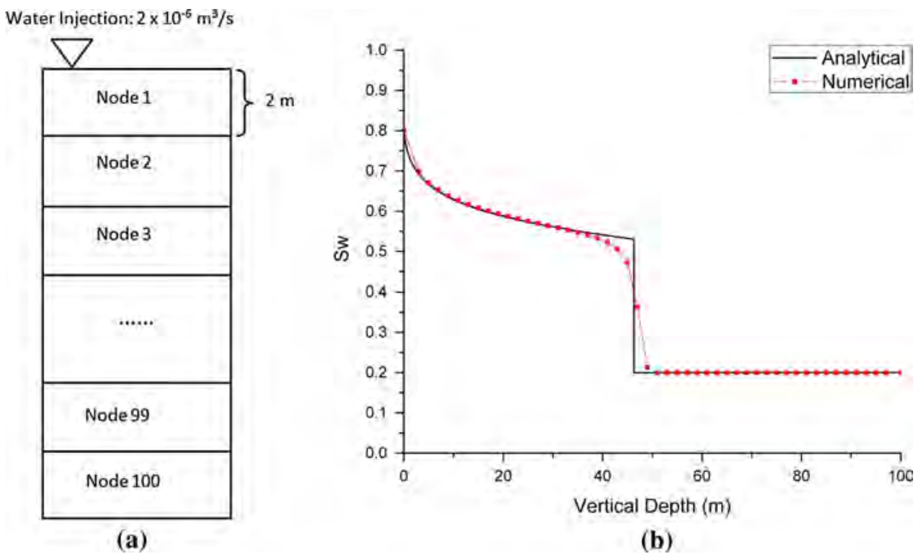

Fig. 5 **a** Simulation model description; **b** Numerical solution against analytical solution

Table 4 Properties of rock and fluid in field study

Parameters	Values	Units
Absolute permeability of matrix	1.0856×10^{-15}	m^2
Absolute permeability of fracture	5.9215×10^{-12}	m^2
Porosity	0.149	
Residual water saturation	0.416	
Residual oil saturation	0.241	
Water viscosity	0.45×10^{-3}	Pa s
Water compressibility	3.5×10^{-10}	Pa
Water density at STC	1000.0	kg/m^3
Oil density at STC	872.4	kg/m^3
Initial bubble point pressure	8.0	MPa
Initial reservoir pressure	32.21	MPa
Initial oil saturation	0.535	

Table 5 Water–oil relative permeability and capillary pressure

S_w	K_{rw}	K_{ro}	P_{cow} (Pa)
0.416	0	1	5.57E+04
0.45	0.032	0.531	8.70E+03
0.485	0.063	0.26	8.00E+03
0.519	0.094	0.12	7.20E+03
0.553	0.127	0.06	6.50E+03
0.587	0.164	0.04	5.90E+03
0.622	0.207	0.022	5.00E+03
0.656	0.258	0.013	4.20E+03
0.69	0.318	0.006	3.40E+03
0.724	0.39	0.003	2.80E+03
0.759	0.475	0	2.40E+03

6 Field Study

This section presents a field example studied with the developed numerical model, which mainly address a multi-stage hydraulic fractured well in a tight oil reservoir. In addition to non-Darcy flow, we also approximately include the rock compaction effect by including pore-pressure-dependent porosity and transmissibility multiplier.

7 Reservoir and Well Description

The reservoir and well data are taken from a real tight oil reservoir in China with properties of rock and fluid shown in Table 4.

The entire simulation is above bubble point pressure without gas phase. The water–oil two-phase relative permeability and capillary pressure data shown in Table 5 are used for the simulation. As mentioned above, the porosity and transmissibility are functions of pore pressures due to rock compaction. The correlations between multipliers and pore pressure

Table 6 Multipliers of porosity and transmissibility

Pore pressure	Porosity multiplier	Transmissibility multiplier
1.00E+05	0.9031	0.01
7.00E+06	0.92656	0.105
1.47E+07	0.95274	0.335
1.97E+07	0.96974	0.381
2.37E+07	0.98334	0.451
2.61E+07	0.9915	0.504
2.77E+07	0.9955	0.584
2.97E+07	0.9975	0.681
3.12E+07	0.999	0.867
3.22E+07	1.000	1.00

Table 7 Reservoir PVT properties

Pressure (Pa)	Bo (rm^3/stc-m^3)	Rs (m^3/m^3)	Oil viscosity (Pa s)
1.00E+05	1	0	1.78E−03
7.00E+06	1.215	55.462	1.68E−03
8.00E+06	1.246	63.5	1.58E−03
3.22E+07	1.231	63.5	1.88E−03
5.00E+07	1.22	63.5	2.11E−03

Table 8 Non-Darcy parameters

Parameters	Water	Oil
δ_D	0.35	0.35
c_ϕ	4.4	4.4
Nonlinear exponent	4.0	4.0

shown in Table 6 are inputted to the simulation; and table 7 lists the PVT properties used in the simulation. The non-Darcy flow parameters used in this field case are included in Table 8.

The simulation domain has a length of 1894 m (x), width of 904 m (y) and thickness of 13 m (z) and is divided into 104 × 47 × 5 with total number of 24,440 grid blocks. There are 12 stages hydraulic fractures for this horizontal well. The size of a general grid block is 20 m, while the fracture node is 2 m. Figure 6 shows the mesh of simulation domain, and Fig. 7 demonstrates the lengths of 12 hydraulic fractures in x–y plane.

8 Simulation Results and Discussion

With above reservoir properties and simulation input, the numerical model is ready to run by setting proper production mechanism. The production is controlled with constant wellbore pressure 8.2 MPa, which is above bubble point pressure 8.0 MPa, to maintain water and oil two-phase flow production. Two simulation runs, Darcy fluid flow and non-Darcy fluid flow, are performed and compared to demonstrate the non-Darcy effect on the productions. Table 9 summarizes the comparison of critical values of the two simulation runs. The main difference is that Darcy model gives more accumulated production, because the non-Darcy

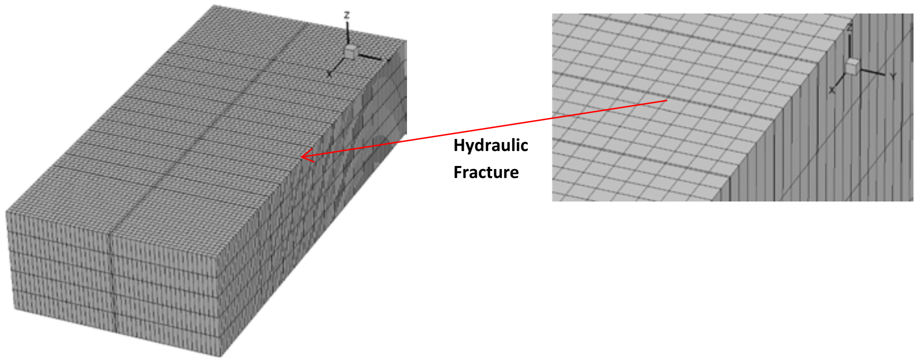

Fig. 6 Grid blocks of simulation domain

Fig. 7 The length and shape of 12 stages of hydraulic fractures

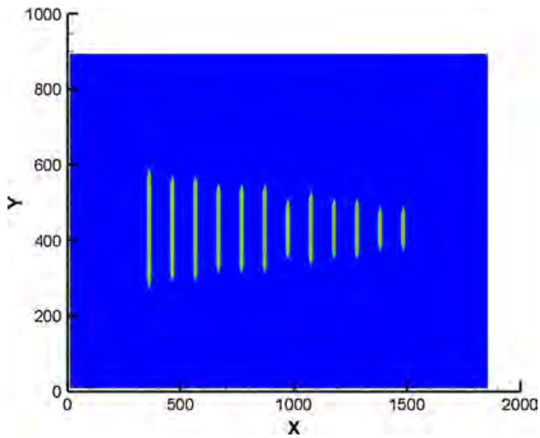

coefficient reduces production rate. Accordingly, non-Darcy model has higher reservoir pressure. Figures 8 and 9 present the accumulated production and volumetric reservoir pressure throughout the simulation, respectively.

From Figs. 8 and 9, it is shown that the simulation results of the two models overlap at the beginning because the non-Darcy flow model is equivalent with Darcy flow at high pressure gradient. After about 10 years' simulation, the non-Darcy flow presents different behaviors from Darcy flow due to larger value of non-Darcy coefficient at low pressure gradient. In other words, the low-velocity non-Darcy effect is non-negligible at the middle and end phases of field production, when the pressure gradient becomes small.

Figures 10, 11, and12 present a variety of comparisons of contour diagram under Darcy and non-Darcy fluid flow at the end of 70-year production. Although the water and oil saturations are very close in the two models, the saturation close to the fractures shows larger differences that Darcy model has much lower oil saturation and higher water saturation; this is because the areas close to hydraulic fractures have small pressure gradient and therefore show larger non-Darcy effect. The reservoir pressure, shown in Fig. 12, has similar pattern in the two models. The pressure close to fractures is much lower than in other areas, and the non-Darcy model shows a general higher reservoir pressure than Darcy model due to less surface production.

Table 9 Comparison of critical values after 70 years simulation

Values	Darcy model	Non-Darcy model
Initial gas volume (st-m^3)	9.008×10^7	9.008×10^7
Initial water volume (st-m^3)	1.531×10^6	1.531×10^6
Initial oil volume (st-m^3)	1.419×10^6	1.419×10^6
Accumulated gas production (st-m^3)	8.435×10^6	8.035×10^6
Accumulated water production (st-m^3)	8.517×10^4	8.124×10^4
Accumulated oil production (st-m^3)	1.328×10^5	1.265×10^5
Volumetric average reservoir pressure (MPa)	8.971	9.921
Volumetric average water saturation	0.4744	0.4738
Volumetric average oil saturation	0.5256	0.5262

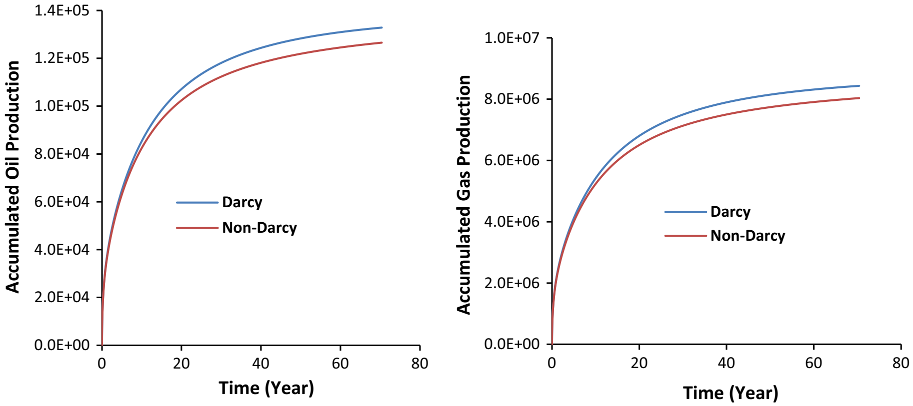

Fig. 8 Comparison of accumulated oil and gas production

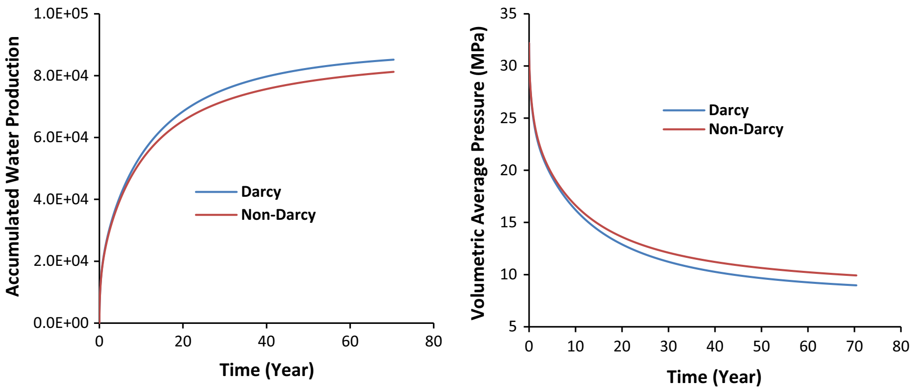

Fig. 9 Comparison of accumulated water production and reservoir pressure

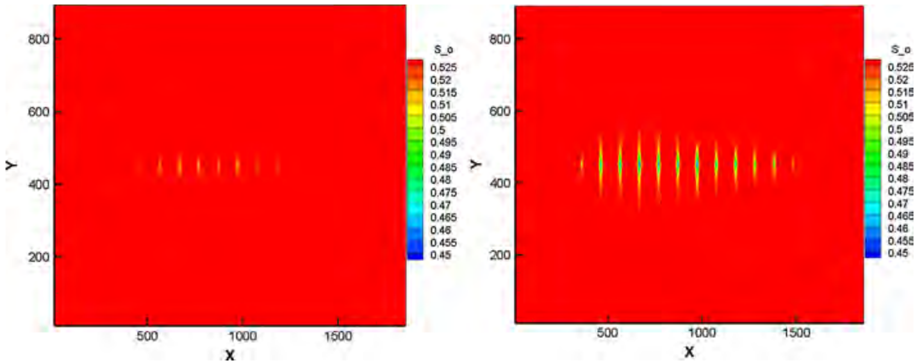

Fig. 10 Oil Saturation of non-Darcy flow model (*left*) and Darcy flow model (*right*)

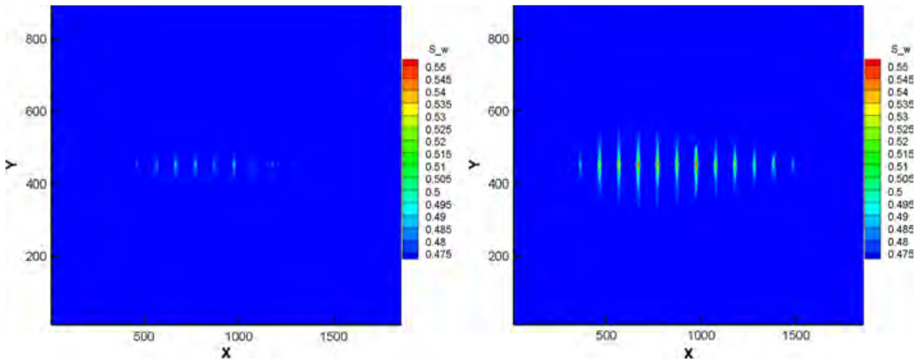

Fig. 11 Water saturation of non-Darcy flow model (*left*) and Darcy flow model (*right*)

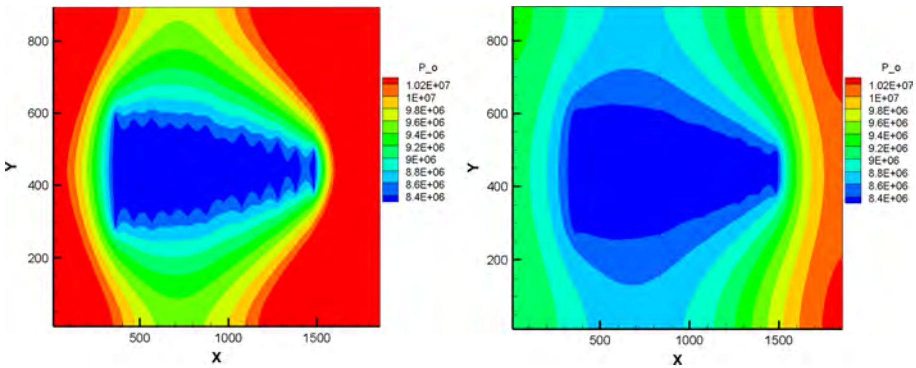

Fig. 12 Reservoir pressure of non-Darcy flow model (*left*) and Darcy flow model (*right*)

This field example has reservoir permeability at 1.1 mD; we expect a much higher non-Darcy effect in a tighter oil reservoir with even lower permeability. For example, three major tight formations in U.S. Bakken, Eagle Ford and Permian, usually have matrix permeability ranging from 10^{-5} md to 10^{-3} md (Wang et al. 2015; Xiong 2015); therefore, non-Darcy effect, induced by boundary layer of flow, could be significantly larger than the field study example above.

9 Conclusions

This paper presents an experiment-based non-Darcy fluid model for low-velocity flow in tight rock reservoirs. We observe a pressure gradient-dependent boundary layer for the flow in a small capillary tube, further derive a single-phase non-Darcy flow equation with two nonlinear parameters, coefficient c_β and dimensionless boundary of flow δ_{D}. In addition, we analyze the non-Darcy effect for multiphase flow and performed an experimental study, which shows the phase-independent δ_{D}. Our multiphase non-Darcy equation provides a single formulation describing both Darcy and non-Darcy behaviors, where non-Darcy flow is only noticeable at a small pressure gradient.

Buckley–Leverett solutions are derived for this non-Darcy flow model for a variety of dimensionless boundary of flow δ_{D}. This non-Darcy flow model has been successfully incorporated into a mature black oil reservoir simulator, MSFLOW, and the numerical implementation is verified with analytical solution. A real field study is then performed with the developed numerical model. The following conclusions are reached from the analysis of analytical solutions and numerical study:

- Analytical solutions show that this low-velocity non-Darcy flow model adversely affects the production performance (larger pressure gradient is required to achieve same flow rate) due to the boundary layer of non-flowable fluids in a tight porous medium.
- The non-Darcy flow model has same simulation results as Darcy flow at the early of production due to negligible non-Darcy coefficient under large pressure gradient. On the other hand, the non-Darcy flow behaviors are more obvious at the end of production due to large non-Darcy coefficients under low pressure gradient.
- The Darcy flow model gives about 5% larger accumulated production of oil and gas, while non-Darcy flow model has about 10% higher reservoir pressure at end of 70 years' simulation for the reservoir with 1.1 mD permeability. We expect a much larger non-Darcy effect on production for a typical tight oil reservoir in USA with matrix permeability at 10^{-5} to 10^{-3} mD.
- A larger decrease in transmissibility occurs in Darcy than in non-Darcy flow due to 10% lower reservoir pressure. Thus, Darcy flow could present higher accumulated production than the simulated results if there is no compaction (transmissibility multiplier) effect included. In the other words, compaction effect weakens the production difference between Darcy and non-Darcy flow models.
- The field example shows that two-phase production accounts for only 10% recovery of oil in place; three-phase simulation is required to study the ultimate recovery. Therefore, further study on boundary-induced non-Darcy effect is recommended for three-phase coexisting fluid system.

Appendix: Experimental Setup and Procedure

The experimental method and setup is the same as the work of Xu and Yue (2007), and the experimental apparatus is shown in Fig. 13.

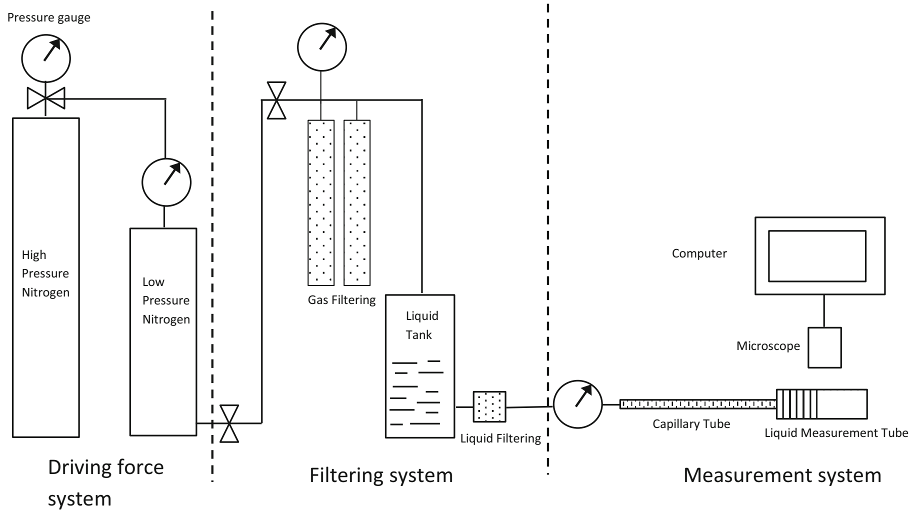

Fig. 13 Experimental setup. Modified according to Xu and Yue (2007)

It consists of three parts, driving force system, filtering system and measurement system. They are separated by the dash lines in the sketch of experimental setup as shown in Fig. 13. Pressurized nitrogen gas is used as the driving force. It is filtered in the gas filtering system and reaches to liquid tank to drive the deionized water in the tank. The moving deionized water is also filtered and reaches to the small capillary tube. The flow rate of capillary tube is measured by observing the change of liquid level in liquid measurement tube and recording the corresponding time. The liquid level is magnified with microscope and transferred to the graphic display in the computer. With the measured flow rate and pressure gradient along the tube, the thickness of boundary flow can be calculated.

References

Ahmed, T.: Reservoir Engineering Handbook. Gulf Professional Publishing, Houston (2006)
Ahmed, T., McKinney, P.: Advanced Reservoir Engineering. Gulf Professional Publishing, Houston (2011)
Aziz, K., Settari, A.: Petroleum Reservoir Simulation. Chapman & Hall, London (1979)
Barree, R.D., Conway, M.W.: Beyond Beta Factors: A Complete Model for Darcy, Forchheimer, and Trans-Forchheimer Flow in Porous Media. Presented at SPE Annual Technical Conference and Exhibition, 26–29 September, Houston, TX (2004)
Buckley, S.E., Leverett, M.C.: Mechanism of fluid displacement in sands. Trans. AIME **146**(01), 107–116 (1942)
Carman, P.C.: Fluid flow through granular beds. Chem. Eng. Res. Des. **75**, 32–48 (1997)
Civan, F.: Implications of alternative macroscopic descriptions illustrated by general balance and continuity equations. J. Porous Media **5**(4), 271–282 (2002)
Civan, F.: Generalized Darcy's law by control volume analysis including capillary and orifice effects. J. Can. Petrol. Technol. **47**(10), 1–7 (2008)
Civan, F.: Comparison of control volume analysis and porous media averaging for formulation of porous media transport. In: Ferreira, J.A., Barbeiro, S., Pena, G., Wheeler, M.F. (eds.) Chapter 2 in Modeling and Simulation in Fluid Dynamics in Porous Media, Series: Springer Proceedings in Mathematics & Statistics, vol. 28, pp. 27–53. Springer, New York, New York (2013)
Darcy, H.: Les Fontaines Publiques de la Ville de Dijon. Dalmont, Paris (1856)
Ergun, S.: Fluid flow through packed columns. Chem. Eng. Prog. **48**, 89–94 (1952)

Evans, R.D., Hudson, C.S., Greenlee, J.E.: The effect of an immobile liquid saturation on the non-Darcy flow coefficient in porous media. SPE Prod. Eng. **2**(4), 331–338 (1987)
Evans, E.V., Evans, R.D.: Influence of an immobile or mobile saturation on non-Darcy compressible flow of real gases in propped fractures. J. Pet. Technol. **40**(10), 1343–1351 (1988)
Forchheimer, P.: Wasserbewegung durch boden. Z. Ver. Deutsch. **45**(1782), 1788 (1901)
Gavin, L.: Pre-Darcy flow: a missing piece of the improved oil recovery puzzle? Presented at SPE/DOE Symposium on Improved Oil Recovery, Tulsa, Oklahoma, 17–21 April (2004)
Hansbo, S.: Consolidation of clay with special reference to influence of vertical drain. Proc. R. Swed. Geotech. Inst. **18**(1), 1–160 (1960)
Hansbo, S.: Consolidation equation valid for both Darcian and non-Darcian flow. Géotechnique **51**(1), 51–54 (2001)
Huang, Y., Yang, Z., He, Y., Wang, X., Luo, Y.: Nonlinear porous flow in low permeability porous media. Mech. Eng. **35**(5), 1–8 (2013)
Jiang, R., Yang, R., Ma, Y., Zhuang, Y., Li, L.: Nonlinear percolation theory and numerical simulation in low permeability reservoirs. Chin. J. Hydrodyn. **26**(4), 444–452 (2011)
Liu, H.H.: Non-Darcian flow in low-permeability media: key issues related to geological disposal of high-level nuclear waste in shale formations. Hydrogeol. J. **22**(7), 1525–1534 (2014)
Liu, H.H., Lai, B., Chen, J.: Unconventional spontaneous imbibition into Shale matrix: theory and a methodology to determine relevant parameters. Transp. Porous Media **111**(1), 41–57 (2015)
Montillet, A.: Flow through a finite packed bed of spheres: a note on the limit of applicability of the Forchheimer-type equation. J. Fluids Eng. **126**(1), 139–143 (2004)
Narasimhan, T.N., Witherspoon, P.A.: An integrated finite difference method for analyzing fluid flow in porous media. Water Resour. Res. **12**(1), 57–64 (1976)
Prada, A., Civan, F.: Modification of Darcy's law for the threshold pressure gradient. J. Pet. Sci. Eng. **22**(4), 237–240 (1999)
Pruess, K.: TOUGH2: A General-Purpose Numerical Simulator for Multiphase Fluid and Heat Flow. Lawrence Berkeley Lab, Berkeley (1991)
Swartzendruber, D.: Non-Darcy flow behavior in liquid-saturated porous media. J. Geophys. Res. **67**(13), 5205–5213 (1962)
Wang, C., Wu, Y.S., Xiong, Y., Winterfeld, P.H., Huang., Z.: Geomechanics Coupling Simulation of Fracture Closure and Its Influence on Gas Production in Shale Gas Reservoirs. Presented at SPE Reservoir Simulation Symposium, Houston, Texas, 23–25 February (2015)
Wu, Y. S.: MSFLOW: Multiphase Subsurface Flow Model of Oil, Gas and Water in Porous and Fractured Media with Water Shut-Off Capability, DOCUMENTATION and User's Guide (1998)
Wu, Y.S.: Non-Darcy displacement of immiscible fluids in porous media. Water Resour. Res. **37**(12), 2943–2950 (2001)
Wu, Y.S., Fakcharoenphol P., Zhang R.: Non-Darcy Displacement in Linear Composite and Radial Flow Porous Media. Presented at SPE EUROPEC/EAGE Annual Conference and Exhibition, Barcelona, Spain, 14–17 June (2010)
Wu, Y.S., Xiong Y., Kazemi H.: Coupled thermo-hydrological processes in enhanced geothermal systems. In: Pore Scale Phenomena: Frontiers in Energy and Environment, pp. 279–298. World Scientific (2015)
Xiong, Y., Fakcharoenphol, P., Winterfeld, P., Zhang, R., Wu, Y.S.: Coupled Geomechanical and Reactive Geochemical Model for Fluid and Heat Flow: Application for Enhanced Geothermal Reservoir. Presented at SPE Reservoir Characterization and Simulation Conference and Exhibition, SPE, Abu Dhabi, UAE, 16–18 September (2013)
Xiong, Y.: Development of a compositional model fully coupled with geomechanics and its application to tight oil reservoir simulation. Ph.D. dissertation, Colorado School of Mines (2015)
Xu, S., Yue, X.: Experimental research on nonlinear flow characteristics at low velocity. J. China Univ. Pet. (Ed. Nat. Sci.) **5**, 014 (2007)
Zeng, B., Cheng, L., Li, C.: Low velocity non-linear flow in ultra-low permeability reservoir. J. Pet. Sci. Eng. **80**(1), 1–6 (2011)
Zhang, R., Wu, Y.S., Fakcharoenphol, P.: Non-Darcy displacement in linear composite and radial aquifer during CO_2 sequestration. Int. J. Oil Gas Coal Technol. **7**(3), 244–262 (2014)